J|A|C|S
ARTICLES
Published on Web 05/05/2007

Short, Highly Ordered, Single-Walled Mixed-Oxide Nanotubes Assemble from Amorphous Nanoparticles

Sanjoy Mukherjee, Keesuk Kim, and Sankar Nair*

Contribution from the School of Chemical & Biomolecular Engineering, Georgia Institute of Technology, 311 Ferst Drive NW, Atlanta, Georgia 30332-0100

Received January 7, 2007; E-mail: sankar.nair@chbe.gatech.edu

Abstract: Nanotubes are important "building block" materials for nanotechnology, but a synthesis process for short (sub-100-nm) solid-state nanotubes with structural order and monodisperse diameter has remained elusive. To achieve this goal, it is critical to possess a definitive mechanistic framework for control over nanotube dimensions and structure. Here we employ solution-phase and solid-state characterization tools to elucidate such a mechanism, particularly that governing the formation of short (~20 nm), ordered, monodisperse (3.3 nm diameter), aluminum-germanium-hydroxide ("aluminogermanate") nanotubes in aqueous solution. Dynamic light scattering (DLS), vibrational spectroscopy, and electron microscopy show that pH-control of chemical speciation in the aluminogermanate precursor solution is important for producing nanotubes. A combination of DLS, UV−vis spectroscopy, and synthesis variations is then used to study the nanotube growth process as a function of temperature and time, revealing the initial condensation of amorphous nanoparticles of size ~6 nm and their transformation into ordered aluminogermanate nanotubes. The main kinetic trends in the experimental data can be well reproduced by a two-step mathematical model. From these investigations, the central phenomena underlying the mechanism are enumerated as: (1) the generation (*via* pH control) of a precursor solution containing aluminate and germanate precursors chemically bonded to each other, (2) the formation of amorphous nanoscale (~6 nm) condensates *via* temperature control, and (3) the self-assembly of short nanotubes from the amorphous nanoscale condensates. This mechanism provides a model for controlled low-temperature (<373 K) assembly of short, monodisperse, structurally ordered nanotube objects.

Introduction

Nanotubes have generated a great deal of interest due to their novel properties and potential use in electronics, photonics, separations, catalysis, and biotechnology[1−5] among other applications. Carbon nanotubes[6,7] and their inorganic analogues (e.g., boron nitride and tungsten disulfide nanotubes)[8−10] continue to be extensively studied, whereas inorganic oxide nanotubes[8,11−15] are emerging as attractive materials due to their potentially wide range of tunable compositions and properties accessible by low-temperature solution-phase chemistry. An important goal of nanotube science and technology is the development of a low-temperature synthetic process with precise control (at sub-100-nm length scale and sub-10-nm diameter scale) over nanotube dimensions to produce "three-dimensionally nanoscale" nanotube objects.[7,16] This would allow the most advantageous exploitation of many of their unique properties (e.g., tunable band gaps, ballistic transport of charge/heat/mass, and quantum confinement phenomena) that manifest themselves strongly at these small length scales.

Although no general strategy has thus far been proposed toward achieving this goal, we are interested in a unique model system that offers mechanistic insights into the assembly of nanotubular objects that could lead to a more general synthesis process. In particular, we consider the single-walled aluminogermanate nanotube,[15,17] which is a synthetic derivative of the aluminosilicate nanotube mineral imogolite.[17−20] This nanotube has a wall structure identical to a layer of aluminum (III) hydroxide (gibbsite), with isolated germanol (≡Ge−OH) groups bound on the inner wall. The nanotube has a highly ordered wall structure composed of six-membered aluminum hydroxide

(1) Avouris, P. *Acc. Chem. Res.* **2002**, *35*(12), 1026−1034.
(2) Balasubramanian, K.; Burghard, M. *Anal. Bioanal. Chem.* **2006**, *385*(3), 452−468.
(3) Baughman, R. H.; Zakhidov, A. A.; de Heer, W. A. *Science* **2002**, *297*(5582), 787−792.
(4) Bianco, A.; Kostarelos, K.; Prato, M. *Curr. Opin. Chem. Biol.* **2005**, *9*(6), 674−679.
(5) Dresselhaus, M. S. *Nature* **2004**, *432*(7020), 959−960.
(6) Iijima, S. *Nature* **1991**, *354*(6348), 56−58.
(7) Dresselhaus, M. S.; Dai, H. *MRS Bulletin* **2004**, *29*(4), 237−239.
(8) Rao, C. N. R.; Nath, M. *Dalton Trans.* **2003**, *1*, 1−24.
(9) Tenne, R. *Angew. Chem. Int Ed.* **2003**, *42*(42), 5124−5132.
(10) Rosentsveig, R.; Margolin, A.; Feldman, Y.; Popovitz-Biro, R.; Tenne, R. *Chem. Mater.* **2002**, *14*(2), 471−473.
(11) Goldberger, J.; Fan, R.; Yang, P. D. *Acc. Chem. Res.* **2006**, *39*(4), 239−248.
(12) Remskar, M. *Adv. Mater.* **2004**, *16*(17), 1497−1504.
(13) Tenne, R.; Rao, C. N. R. *Philos. Trans. R. Soc. London, Ser. A* **2004**, *362*(1823), 2099−2125.
(14) Xiong, Y. J.; Mayers, B. T.; Xia, Y. N. *Chem. Commun.* **2005**, *40*, 5013−5022.
(15) Mukherjee, S.; Bartlow, V. A.; Nair, S. *Chem. Mater.* **2005**, *17*(20), 4900−4909.
(16) Tenne, R. *Nature Nanotechnol.* **2006**, *1*(2), 103−111.
(17) Wada, S.; Wada, K. *Clays Clay Miner.* **1982**, *30*(2), 123−128.
(18) Cradwick, P. D.; Wada, K.; Russell, J. D.; Yoshinaga, N.; Masson, C. R.; Farmer, V. C. *Nat. Phys. Sci.* **1972**, *240*(104), 187−188.
(19) Russel, J. D.; McHardy, W. J.; Fraser, A. R. *Clay Miner.* **1969**, *8*, 87−99.
(20) Wada, K.; Yoshinaga, N. *Am. Mineral.* **1969**, *54*(1−2), 50−57.

10.1021/ja070124c CCC: $37.00

rings, a repeat unit of 0.85 nm along the nanotube axis, and an outer diameter of 3.3 nm.[15] The empirical formula is $(OH)_3Al_2O_3$-GeOH. In our previous phenomenological study,[15] we observed the puzzling fact that the nanotube size (~20 nm) did not appear to change appreciably during several days of synthesis time, whereas the concentration of nanotubes appeared to increase substantially (as evinced by X-ray diffraction from dried reaction products). This indicated a fundamental and important difference between the present system and the conventional routes[12,21,22] for nanotube growth. In the latter cases, growth occurs by catalytic addition of molecular or atomic precursors to the ends of the nanotube to produce long (~ 1 μm) carbon/BN/WS_2 nanotubes, or it may occur by a combination of crystal nucleation, growth and organic templating effects (during liquid-phase growth) to produce long, multiwalled oxide nanotubes. In the above works, the use of organic-templating strategies have not yielded single-walled nanotubes, e.g., templated metal oxide nanotubes are multiwalled and are several tens of nanometers in outer diameter.

Here we report our investigation that establishes the main aspects of a novel nanotube formation mechanism. Because the aluminogermanate nanotube synthesis proceeds over a time scale of days to weeks, we were able to employ a number of solution-phase (dynamic light scattering and UV−vis absorbance spectroscopy) and solid-state (vibrational spectroscopy and electron diffraction) characterization tools. After careful interpretation of all available evidence, we are in a position to elucidate a mechanism for the self-assembly of short, highly ordered nanotube materials. The mechanism clearly suggests a route to nanotube materials of small (sub-100-nm) and controllable dimensions. This route consists of controlling chemical bonding between precursors in solution *via* pH control, followed by the use of temperature control to form nanoparticle condensates, which sets the stage for self-assembly processes that work to assemble small, ordered objects from the amorphous condensate.

Experimental Section

Nanotube Synthesis. Tetraethylorthogermanate (TEOG) was added dropwise to a stirred solution of 2.5 millimolar (mM) aluminum chloride ($AlCl_3$) solution until the Al:Ge ratio was 1.8 and left to stand for 45 min under vigorous stirring. Then a 0.1 M NaOH solution was added at the rate of 0.3 mL/minute until the pH of the solution reached 5.0. The pH was brought down immediately to 4.5 by dropwise addition of a solution containing 0.1 M HCl and 0.2 M acetic acid. The resulting clear solution was allowed to stir for 3 h and then reacted under reflux conditions at different temperatures, as described in the following sections.

Characterization Methods. For DLS and UV−vis analyses, 5 mL samples were withdrawn from the reactor and filtered through a 0.2 μm pore size syringe filter to produce a dust-free sample containing only nanoparticles. DLS data were collected with a Wyatt DAWN EOS instrument. The scattering angle was 108° and the wavelength of the laser was 690 nm. The autocorrelator delay time (τ) was 1 μs. A series of 120 scans were performed on the sample, each with a 1-second acquisition time. UV−vis data was obtained on a HP 8453 UV−vis spectrophotometer. A quartz cuvette was used as a sample holder because it is optically transparent to UV radiation. FT-Raman and FT-IR were performed on freeze-dried samples. Liquid samples (100 mL) were taken directly from the reactor and immediately frozen at −20 °C before application of vacuum. FT-Raman spectra were obtained on a Bruker IFS-66/FRA-106 instrument operating with a Nd:YAG laser. FT-IR spectra were collected under vacuum conditions on a Bruker IFS 66v/S spectrometer. At least 2048 scans were collected for each FT-Raman and FT-IR spectrum, with a resolution of 8 cm^{-1}. Other qualitative characterizations (TEM and electron diffraction) were carried out with a JEOL 100CX TEM operating at 100 kV. X-ray diffraction characterization was carried out with a PANalytical X'Pert Pro instrument operating with a Cu Kα wavelength (0.154 nm).

Results and Discussion

Control of Chemical Bonding in the Precursor Solution. The established synthesis process[15,17] (also see Experimental Section) can be divided into five steps, all carried out under vigorous stirring: (I) *Hydrolysis*, i.e. dissolution of aluminum and germanium precursors in water at pH ~3.5, (II) *Basification*, i.e. slow ramping of the pH to 5.0 by addition of sodium hydroxide, (III) *Partial Re-acidification* to pH 4.5 by addition of acid, (IV) *Equilibration* at room temperature, and (V) *Heating* above room temperature under reflux conditions. Steps I, IV, and V are common in the synthesis of inorganic oxide materials. However, Steps II and III are unusual and have no explanation in the literature, though they were empirically found to be necessary for the formation of nanotubes rather than dense crystalline or amorphous materials.[23,24] Indeed, we also found that successful nanotube synthesis—though completely reproducible—was critically dependent on the correct execution of the sequence of Steps I−V.

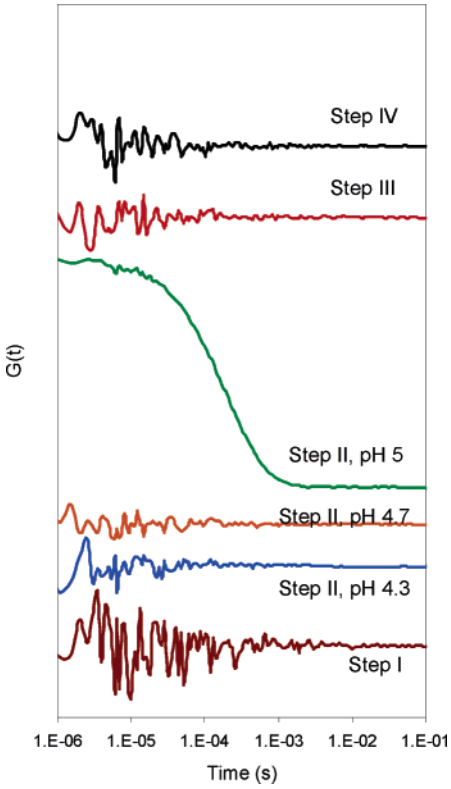

Figure 1. Autocorrelation functions $G(t)$ obtained from dynamic light scattering during Steps I−IV of nanotube synthesis.

It was first verified (see Supporting Information) that carrying out the synthesis with omission of Steps II and III results in the formation of dense crystalline boehmite (aluminum oxyhy-

(21) Little, R. B. *J. Cluster Sci.* **2003**, *14*(2), 135−185.
(22) Zhu, Y. Q.; Hsu, W. K.; Terrones, H.; Grobert, N.; Chang, B. H.; Terrones, M.; Wei, B. Q.; Kroto, H. W.; Walton, D. R. M.; Boothroyd, C. B.; Kinloch, I.; Chen, G. Z.; Windle, A. H.; Fray, D. J. *J. Mater. Chem.* **2000**, *10*(11), 2570−2577.

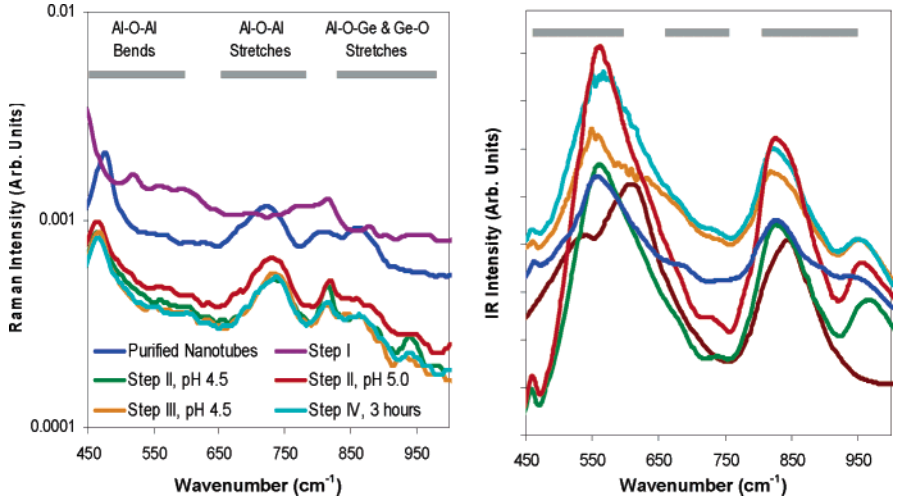

Figure 2. (a) Raman spectra of freeze-dried samples during Steps I−IV and the purified nanotube product. (b) Infrared spectra of the same samples. The legend for both parts is the same. Important vibrational band regions are labeled identically in both parts and are discussed in the text.

droxide, AlOOH) irrespective of the presence of germanium. This evidence indicated that Steps II and III facilitate a controlled chemical interaction between aluminum and germanium precursors that enables the formation of aluminogermanate nanotubes in Step V. To study the events occurring during Steps I−IV in more detail, we first used dynamic light scattering (DLS) to probe nanoparticle evolution during these steps. DLS was found to be preferable over small-angle X-ray scattering, because the latter gives a very weak signal at the nanoparticle concentrations of interest (1−10 μM). Figure 1 shows DLS autocorrelation functions of liquid samples from the reactor at various stages. These experiments have been reproduced several times to ensure their validity. Complete dissolution of precursors (i.e., lack of nanoparticles) in Step I is evinced by the flat autocorrelation function. Upon increasing the pH (Step II), no nanoparticles are detected until the pH reaches 5, whereupon a well-defined autocorrelation function appears corresponding to nanoparticle condensates 20 nm in size. However, these nanoparticles quickly disappear upon partial re-acidification (Step III) and do not reappear during equilibration (Step IV).

We then investigated Steps I−IV in greater detail with Raman and infrared (IR) spectroscopy (Figure 2). As expected, liquid-phase spectroscopy failed to produce sufficient Raman scattering or IR absorption signal at the concentrations of interest. Thus, solid-state spectroscopy was performed on freeze-dried samples removed from the reactor during these four steps. The Raman and IR spectra corroborate the following main points, based on analysis of the 450−1000 cm^{-1} region that is of importance[17] in identifying the aluminogermanate nanotube material. First, the main change in the bonding environment of the precursors is between Steps I and II (i.e., upon basification), whereas there are only minor changes in the vibrational spectra thereafter (through Steps II−IV). Second, the vibrational spectra of the precursors in Steps II−IV are very similar to that of the purified nanotubes obtained as the final product of an independent synthesis experiment. In particular, they show that Al−O−Al and Al−O−Ge linkages have been formed with similar Raman and IR frequencies as in the nanotube product, whose vibrational bands have been assigned qualitatively in previous work.[17] The "Al−O−Al bending and stretching" frequency regions, as well as the "Al−O−Ge and Ge−O stretching" frequency regions for the nanotube product are labeled. Note that bands with high Raman intensity usually have low IR intensity and vice versa. For example, the Al−O−Al mode at 450 cm^{-1} is intense in the Raman and weak in the IR spectrum, whereas the modes around 550 cm^{-1} are weak in the Raman and intense in the IR spectrum. Similarly, the Al−O−Al stretching mode at 700 cm^{-1} is intense in Raman and weak in the IR spectrum. The Al−O−Ge and Ge−O stretching bands at 810, 850, and 950 cm^{-1} are relatively weak in the Raman spectrum but more intense in the IR spectrum.

Finally, we used liquid-phase UV−vis spectroscopy to prove that there are no structurally ordered species at any stage of the Steps I−IV. UV−vis spectroscopy is an excellent probe of structural order in oxide materials (also see following sections) and allows us to easily distinguish between ordered nanotubes and amorphous nanoparticles or precursors even at nanomolar concentrations. The UV−vis spectra of the solutions in Steps I−IV are completely featureless, as expected from aqueous solutions of aluminate and germanate precursors (whether monomeric or oligomeric). No ordered materials are observed by TEM, electron diffraction, or XRD on the solid products after freeze-drying. Together, the DLS, Raman, IR, and UV−vis data provide insight on how control of chemical bonding in the precursor solution can influence nanotube synthesis. The role of Step II (basification) is to promote co-condensation of aluminum and germanium precursors into small (subnanometer) aluminogermanate precursors in which the chemical bonding resembles that of the aluminum and germanium atoms in the final nanotube product. The role of Step III (partial re-acidification to pH 4.5) is to prevent precipitation of amorphous materials that begins when basification reaches pH 5 (as evinced by the appearance of nanoparticles in the DLS measurements). Furthermore, our data confirm the existence of only *subnanometer precursors* before temperature changes are applied, save for the temporary appearance of *amorphous nanoparticles* (only in Step II, when pH $\approx$ 5).

Nanotube Formation. Next, we studied the formation of nanotubes during Step V, as a function of reaction time (up to

(23) Barrett, S. M.; Budd, P. M.; Price, C. *Eur. Polym. J.* **1991**, *27*(7), 609−612.
(24) Ackerman, W. C.; Smith, D. M.; Huling, J. C.; Kim, Y. W.; Bailey, J. K.; Brinker, C. J. *Langmuir* **1993**, *9*(4), 1051−1057.

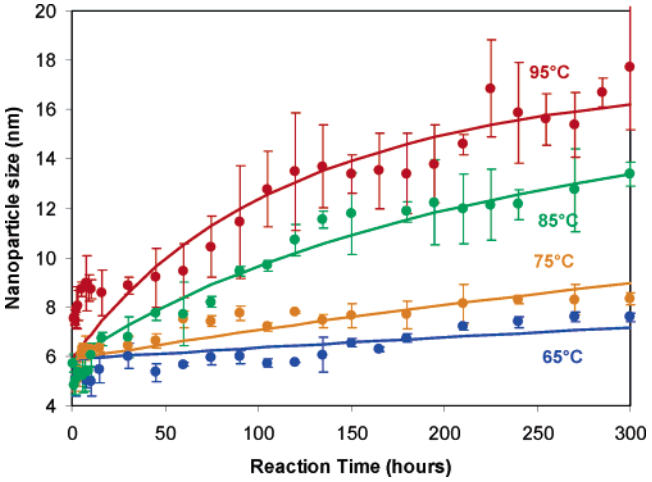

Figure 3. Average nanoparticle size versus time obtained from dynamic light scattering. The closed symbols are experimental data whereas the solid lines are model fits (see discussion).

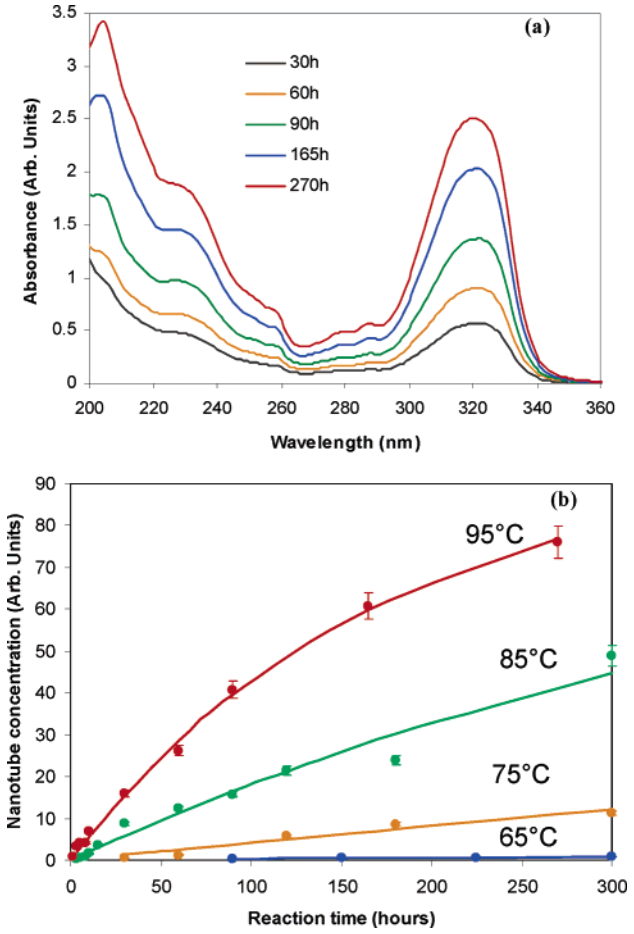

Figure 4. (a) UV−vis spectra of the solution at various times during reaction at 95 °C. (b) Concentration of nanotubes, obtained from the 320 nm excitation as a function of growth time. The closed symbols are experimental data whereas the solid lines are model fits (see discussion).

300 h) and temperature (65 °C-95 °C) in a batch reactor configuration. Additional seeded-batch and semi-batch experiments were carried out at 95 °C. Together, these experiments provide critical information on the nanotube growth mechanism and eliminate other possible models. In each case, multiple experiments were carried out over a total period of more than a year to ensure reproducibility and realistic error estimates on the quantitative measures of nanotube growth. We can quantitatively obtain *average nanoparticle sizes* in the reactor from DLS autocorrelation functions, as well as the *concentration of only nanotubes* from UV−vis absorption intensities. We can also obtain (semiquantitatively) the *total concentration of all nanoparticles* (nanotubular as well as amorphous) from DLS photon scattering signal intensities. Figure 3 shows the average nanoparticle size obtained from DLS as a function of reaction time and reaction temperature. Nanoparticles of size 5−7 nm appear immediately upon heating but do not exist prior to this step. Thereafter, we see a slow increase in the average particle size. The "apparent rate of growth" of the nanoparticles varies from 0.04 nm/hr at 95 °C to 0.001 nm/hr at 65 °C. If interpreted in terms of a model that involves addition of precursors to nanotube ends, this rate of growth is negligible.

Figure 4a shows example UV−vis spectra obtained at 95 °C for different reaction times. The spectra differ only in the intensity of the peaks, which is proportional to the concentration of nanotubes in the solution. The intensity of the peaks increases by more than a factor of 50 during the reaction period, whereas the average nanoparticle size (from DLS) increased by less than a factor of 3 during the same period. Furthermore, these spectra are found to be identical in shape to that of a pure dialyzed aluminogermanate nanotube solution. Using detailed UV−vis data obtained at four temperatures (see Supporting Information), we construct the plot of Figure 4b that shows the evolution of the nanotube concentration as a function of time. The spectra were background-subtracted and then fitted using Gaussian peaks according to procedures described previously.[25] The total area under the 320 nm excitation was used to track the nanotube concentration. This is also the first report of the optical properties of these materials, which are wide band gap semiconductors (with $E_g = 3.6$ eV). The sharp, intense peaks may reveal the presence of confined excitons and other phenomena that are currently of considerable interest in the photonic applications of nanoparticles.[25−30] These properties are under detailed study and will be presented in a forthcoming report. Figure 5 shows the photon scattering signal intensity (measured during DLS experiments) as a function of reaction time. The intensity has been normalized by the nanoparticle size (obtained simultaneously from the DLS autocorrelation function). This is because the intensity is proportional to the product of the concentration and the molecular weight (which in the case of a 1-D nanotube is proportional to its length).[31] Thus, the normalization to the particle size semiquantitatively isolates the contribution from increasing nanotube concentration. As in the case of the UV−vis spectra, the total concentration of nanoparticles in the solution is seen to be increasing substantially with time at higher temperatures of reaction.

(25) Yu, H.; Li, J. B.; Loomis, R. A.; Wang, L. W.; Buhro, W. E. *Nat. Mater.* **2003**, *2*(8), 517−520.
(26) Kan, S.; Mokari, T.; Rothenberg, E.; Banin, U. *Nat. Mater.* **2003**, *2*(3), 155−158.
(27) Steiner, D.; Katz, D.; Millo, O.; Aharoni, A.; Kan, S.; Mokari, T.; Banin, U. *Nano Lett.* **2004**, *4*(6), 1073−1077.
(28) Chen, S. J.; Liu, Y. C.; Shao, C. L.; Xu, C. S.; Liu, Y. X.; Liu, C. Y.; Zhang, B. P.; Wang, L.; Liu, B. B.; Zou, G. T. *Appl. Phys. Lett.* **2006**, *8*(13), art #133127.
(29) Wang, F.; Dukovic, G.; Brus, L. E.; Heinz, T. F. *Science* **2005**, *308*(5723), 838−841.
(30) Wirtz, L.; Marini, A.; Rubio, A. *Phys. Rev. Lett.* **2006**, *96*(12), art. #126104.
(31) Wyn, B. *Dynamic Light Scattering: The Method and Some Applications*; Clarendon Press: New York, 1993.

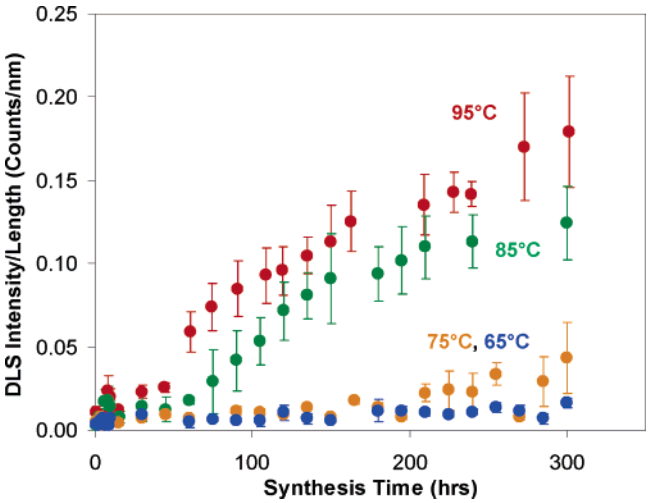

Figure 5. Semiquantitative measurement of total nanoparticle concentration versus time, from dynamic light scattering signal intensity.

Together, Figures 3−5 clearly reveal the central mechanistic aspects of the nanotube growth. The temperature rise at the onset of Step V results in the condensation of Amorphous NanoParticles ("ANPs") of size ∼ 5−7 nm (Figure 3) and low concentration (Figure 5). At the higher reaction temperatures, ordered NanoTubes ("NTs") begin to emerge at an early stage (a few hours) as evinced by the appearance of peaks in UV−vis spectra (Figure 4 and Supporting Information). The UV−vis spectra remain practically the same (except for the increasing intensity) throughout the reaction and result from increasing concentrations of the same ordered material as the reaction proceeds. At the same time, the average nanoparticle size increases slowly over the reaction time of 300 h.

We also carried out other experiments to examine the possibility of growth by NT nucleation in solution followed by addition of dissolved precursors to the NT ends. Figure 6 presents DLS particle sizes measured during seeded-batch and semi-batch experiments at 95 °C in comparison to the batch experiment data. In seeded growth, 5 mL of a suspension of purified NTs (of size 19 nm as obtained by a prior DLS measurement) was added to the reactor at the onset of Step V. The amount of nanotubes added was such that their average length would increase by a factor of 3 during the reaction time if the nanotube formation was dominated by end-growth. However, Figure 6 shows that the particle sizes do not increase substantially, and both the batch and seeded-batch reactions tend to converge to a similar nanoparticle size at long times. The main difference is the initially larger average particle size in the seeded-growth experiment, owing to the addition of NTs at the beginning of Step V. Another important fact is that the nanotube length is not limited by declining precursor concentration in the batch reactor experiments, even as the nanotube concentration continues to increase after long reaction times of 300 h at 95 °C. This point was further verified by a semi-batch experiment, in which reactants were continuously added to the reactor during the synthesis. In this case, the initial concentration of the precursors was the same as in the batch reaction, but the initial volume of solution was only 25 mL. Precursor solution was continuously added to the reactor at a rate of 5 mL/hr. The evolution of the average nanoparticle dimensions measured by DLS (Figure 6) shows no substantial differences from the batch experiments at long times. Finally, the size of the purified NTs (obtained by dialysis of the solution after reaction) was almost constant (at 19 ± 2 nm) irrespective of the growth method (Figure 6). On the basis of all the results, the apparent increase of nanoparticle size during the reaction (as observed in DLS) is not primarily due to the increase in the nanotube length by solution-phase addition of growth units to the ends, but rather due to evolution of the ANPs into low-density (porous), short, ordered NTs by self-assembly as evinced by the UV−vis spectra. Simultaneously, limited aggregation of the ANPs may increase the average nanoparticle size and size distribution. In the next section, we explain the mechanistic implications of the combined DLS and UV−vis studies described above.

Overall Mechanism and a Simple Mathematical Model. We are now in a position to propose a nanotube formation mechanism (Figure 7) that we believe to be conclusive in its essential aspects. The initial Steps I−IV induce the formation of aluminogermanate precursors that are capable of assembly into the nanotube structure. The formation of ANPs from precursors in Step V can be considered (in general) as a reversible reaction. Having excluded the possibility of liquid-phase growth of the NTs, the ANPs (once formed) must be evolving irreversibly into ordered NTs primarily through internal self-assembly as indicated in Figure 7. There is a unique energy minimum in this system as a function of the nanotube diameter,[32,33] which is likely to be important in causing self-assembly into NTs of monodisperse diameter within the confines of the ANPs. Regarding the role of amorphous nanoparticles and their evolution to ordered materials, we also note a remarkable similarity between the nanotube formation mechanism deduced here (following our speculation in a previous work[15]) and the reported mechanisms of nanoporous crystal (zeolite) formation.[34−37] In the latter case, aggregation processes are additionally important for the formation of bulk crystalline materials.[38] On the other hand, the much more dilute concentrations encountered in the nanotube system can be expected to limit the aggregation processes and lead to the formation of nanoscale (rather than bulk) materials. In other words, each NT can be formed from only a few ANPs (and from a minimum of one ANP). One objective of our ongoing investigations is to ascertain quantitatively the role of aggregation that may occur in parallel to the ANP → NT transformation processes. The role of amorphous nanoparticles has also been suggested to be of profound importance in biomineralization at the interface of biological structures with aqueous environments.[39,40] Very recently, pH-influenced condensation has also been shown to influence the formation of dense germanium oxide nanoparticles.[41]

The UV−vis concentration data and the DLS particle size data can be well fitted (Figures 3 and 4b) to a simple two-step

(32) Konduri, S.; Mukherjee, S.; Nair, S. *Phys. Rev. B* **2006**, *74*(3), art #033401.
(33) Tamura, K.; Kawamura, K. *J. Phys. Chem. B* **2002**, *106*(2), 271−278.
(34) Davis, T. M.; Drews, T. O.; Ramanan, H.; He, C.; Dong, J. S.; Schnablegger, H.; Katsoulakis, M. A.; Kokkoli, E.; McCormick, A. V.; Penn, R. L.; Tsapatsis, M. *Nat. Mater.* **2006**, *5*(5), 400−408.
(35) Mintova, S.; Olson, N. H.; Valtchev, V.; Bein, T. *Science* **1999**, 283(5404), 958−960.
(36) Cheng, C. H.; Shantz, D. F. *J. Phys. Chem. B* **2005**, *109*(15), 7266−7274.
(37) Kragten, D. D.; Fedeyko, J. M.; Sawant, K. R.; Rimer, J. D.; Vlachos, D. G.; Lobo, R. F.; Tsapatsis, M. *J. Phys. Chem. B* **2003**, *107*(37), 10006−10016.
(38) Davis, M. E. *Nature* **2002**, *417*(6891), 813−821.
(39) Davis, M. E. *Science* **2004**, *305*(5683), 480−480.
(40) Navrotsky, A. *Proc. Natl. Acad. Sci. U.S.A.* **2004**, *101*(33), 12096−12101.
(41) Rimer, J. D.; Roth, D. D.; Vlachos, D. G.; Lobo, R. F. *Langmuir* **2007**, *23*(5), 2784−2791.

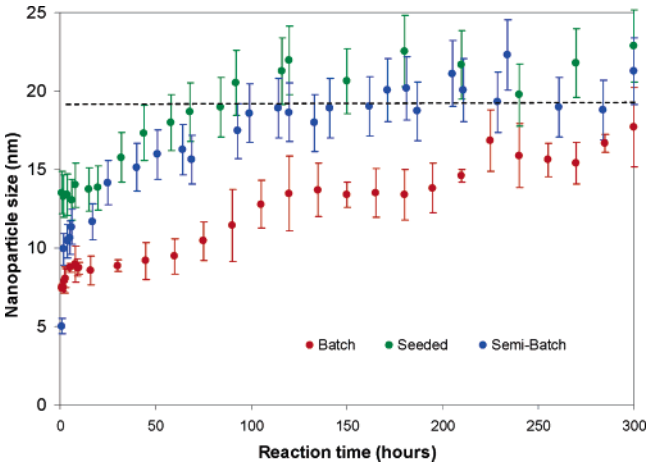

Figure 6. Comparison of DLS nanoparticle sizes obtained from batch, seeded-batch, and semi-batch growth. The dashed line shows the nanoparticle size measured from purified (dialyzed) nanotube products of the three reactions after 300 h.

mathematical model based in Figure 7, which involves reversible first-order formation of ANPs from precursors, followed by irreversible first-order formation of NTs. Note that the ANP evolution to NTs may involve a series of rearrangements (involving hydrolysis and condensation) of atoms within the ANPs, and even limited aggregation of the ANPs. Here, we use bulk concentrations $C_A(t)$ and $C_N(t)$ to represent the concentration of ANPs and the fully evolved NTs respectively. The internal rearrangements, precursor-ANP exchange, and any aggregation processes are represented by effective rate constants shown in Figure 7. Such a "minimalist" model can be used to capture the main features of the nanotube assembly mechanism, and similar models have been applied to describe crystal growth by nanoparticle aggregation.[34,42] A quasi-steady-state assumption is made for the ANP concentration, which remains low throughout the reaction as seen in the experiments carried out at 65 °C and 75 °C (Figure 5). Thus, the model relates the concentrations of the precursors (C_P), ANPs (C_A), and NTs (C_N) through the following three first-order rate equations: $dC_P/dt = -k_1C_P + k_{-1}C_A$; $dC_A/dt = (k_1/N_P)C_P - (k_{-1}/N_P)C_A - k_2C_A$; and $dC_N/dt = k_2C_A$. Here, N_P is the number of precursors condensing into a single ANP. The rate equations can then be integrated analytically, and the resulting $C_A(t)$ and $C_N(t)$ can be used to fit the effective overall rate constant (K) for nanotube formation, as well as that for the ANP → NT transformation (k_2). The QSS approximation ($dC_A/dt \approx 0$) leads to the following three expressions for species concentrations: $C_P(t) = C_{P0}e^{-Kt}$,$C_A(t) = (KC_{P0}/k_2N_P)e^{-Kt}$, and $C_N(t) = (C_{P0}/N_P)(1 - e^{-Kt})$. Here, $K = k_1k_2/(k_{-1}/N_P + k_2)$ is the overall pseudo-first-order rate constant for NT formation and C_{P0} is the initial precursor concentration.

We first fit the measured UV−vis intensity, which is proportional to the NT concentration: $I_{UV} = \alpha_1C_N = \alpha_1'(1 - e^{-Kt})$, where α_1 is the instrumental calibration factor and $\alpha_1' = \alpha_1C_{P0}/N_P$. This fit has only two parameters: K and α_1'. Then we fit the measured average DLS particle size, which at low concentrations is well described by an arithmetic average of the sizes of ANPs (L_A) and NTs (L_N): $\bar{L}_{DLS} = (L_AC_A + L_NC_N)/(C_A + C_N)$. Substituting the model expressions for C_A and C_N, the fit of the DLS particle size over the four temperatures involves three parameters: L_A, L_N, and k_2 (because K is already determined). This simple model captures all the observed trends in the evolution of nanoparticle size and NT concentration. The ANP and NT sizes can be fitted as practically independent of temperature within the range of conditions investigated. The fit results can easily be improved by specifying a temperature-dependent ANP size, although this leads to introduction of a larger number of parameters. Also see Supporting Information for a summary of the fitted values of all the parameters and further discussion of the fit procedure.

The fitted rate constants K and k_2 were well described by Arrhenius expressions to yield the activation energies. The kinetic experiments done at four temperatures yield effective activation energies of 181 ± 6 and 110 ± 7 kJ/mol for K (overall "precursors → NT") and k_2 ("ANP → NT"), respectively (see Supporting Information for further details), which are well within physical possibility for oxide formation.[34,43] The fitted ANP size (5.9 ± 1 nm) and the fully evolved NT length (17.6 ± 3 nm) are in agreement with the DLS and TEM[15] observations of the pure dialyzed materials. As mentioned earlier, the changing particle sizes measured in DLS experiments are not primarily because of an increase in NT length due to solution-phase growth by precursor addition, but rather because the concentration of the (longer) NTs continues to grow in proportion to that of the (compact) ANPs. Hence, the average particle size measured by DLS increases with time.

We further emphasize that the mechanism does not preclude the concurrent role of processes such as aggregation of the ANPs, which would have the effect of increasing the average size (and size distribution) of the ANPs and thus causing an increase in the average length (and length distribution) of the NT that is eventually formed. The possible role of aggregation processes, as well as the effects of parameters such as increasing precursor concentration, are under investigation and are considered to be outside the scope of this paper. However, the central aspect of the mechanism is the discovery that the dissolved nanotube precursors are condensed into amorphous nanoparticles containing localized precursors, thus allowing the assembly of ordered nanotubes of small sizes and whose structure is controlled by the nature of the precursors. This is a novel concept as pertaining to nanotube synthesis, and for the synthesis of highly ordered nanoscale metal oxide objects in general. The application of this mechanism in combination with metal oxide chemistry and variations in parameters such as the ionic strength (which can influence nucleation, growth, and aggregation processes), precursor concentration, and even the solvent, may allow development of more generalized processes based on amorphous nanoparticle condensation and self-assembly to yield very small metal oxide nanotube objects of tunable composition and functionality—a highly desirable goal of nanomaterials science and technology. As illustrated here, such routes could exploit the fact that a large number of metals are well-known to form layered oxides, oxyhydroxides, and hydroxides.[44] Such a tendency can potentially be diverted to induce nanotube formation *via* co-condensing ions (such as germanate, silicate, and phosphate) that alter the chemical bonding and energetics of the system as seen in the current

(42) Drews, T. O.; Katsoulakis, M. A.; Tsapatsis, M. *J. Phys. Chem. B* **2005**, *109*(50), 23879−23887.
(43) Nikolakis, V.; Kokkoli, E.; Tirrell, M.; Tsapatsis, M.; Vlachos, D. G. *Chem. Mater.* **2000**, *12*(3), 845−853.
(44) Jolivet, J.-P. *Metal Oxide Chemistry and Synthesis: From Solution to Solid State*; Wiley: West Sussex, England, 2003.

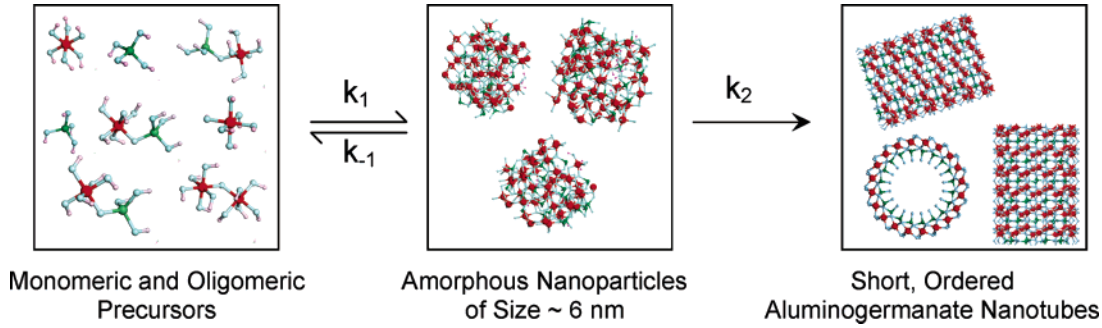

Figure 7. Summary of the aluminogermanate nanotube growth mechanism. Red, aluminum; green, silicon; light blue, oxygen; gray, hydrogen. Solvent (water) molecules are not shown for clarity. Aluminogermanate precursors condense into amorphous nanoparticles which then rearrange into short, ordered nanotubes (see text for details). Note that the equilibrium of the first step is dynamic, i.e., exchange of precursors between ANPs and precursor solution can occur.

synthesis. Furthermore, the fact that the ANPs necessarily contain only a few thousand atoms may allow computational prediction/design of their self-assembly into ordered objects leading to synthesis of new classes of nanomaterials.

Conclusion

We have described the essential mechanistic aspects of a route toward the assembly of very small (∼20 nm), structurally ordered, single-walled aluminogermanate nanotubes in aqueous conditions. A combination of solution phase (dynamic light scattering and UV−vis spectroscopy) and solid phase (Raman, FTIR, electron diffraction, TEM) characterization methods with necessary variations of the basic synthesis process, allows us to propose a concrete mechanism for this process which is of importance toward the goal of synthesizing small, ordered, metal oxide nanotubes and related nanomaterials. In particular, our investigation leads to a mechanism that involves first the use of pH control to generate aluminogermanate precursors with appropriate chemical bonding conducive to assembly into nanotubes, followed by the use of temperature control (at 65−95 °C) to condense these precursors into amorphous nanoparticles (ANPs) of size ∼6 nm, and finally the self-assembly of short, ordered aluminogermanate nanotubes (NTs) of size ∼20 nm from these amorphous condensates. A two-step kinetic model of this process can capture the main features of the mechanism, *viz.* increasing NT concentration and slowly changing average nanoparticle size, both of which are due to the ANP → NT transformation.

Acknowledgment. We acknowledge financial support from the ACS Petroleum Research Fund (#44074-G10) and the Georgia Institute of Technology. We also acknowledge access to spectroscopic instrumentation (UV−vis, Raman, and IR) in the laboratories of C. A. Eckert and C. W. Jones.

Supporting Information Available: TEM image and electron diffraction pattern of synthesis product in absence of germanium, complete UV−vis spectra for nanotube syntheses at four temperatures, table of fitted kinetic model parameters, and Arrhenius plot of rate constants with extracted activation energies. This material is available free of charge via the Internet at http://pubs.acs.org.

JA070124C